JMEPEG (2013) 22:3228–3236
DOI: 10.1007/s11665-013-0635-7

1059-9495/$19.00

Effects of Crimping on Mechanical Performance of Nitinol Stent Designed for Femoral Artery: Finite Element Analysis

F. Nematzadeh and S.K. Sadrnezhaad

(Submitted February 25, 2012; in revised form March 29, 2013; published online July 9, 2013)

Nitinol stents are used to minimize improper dynamic behavior, low twistability, and inadequate radial mechanical strength of femoral artery stents. In this study, finite element method is used to investigate the effect of crimping and Austenite finish temperature (A_f) of Nitinol on mechanical performance of Z-shaped open-cell femoral stent under crimping conditions. Results show that low A_f Nitinol has better mechanical and clinical performance due to small chronic outward force, large radial resistive force, and appropriate superelastic behavior.

Keywords crimping, femoral artery, finite element analysis, mechanical performance, Nitinol stent

1. Introduction

Stenosis superficial femoral artery (SFA) is a well-known disease related to vascular tissue (Ref 1). The application of stent is a good way to solve this problem (Ref 2). Previous studies have dealt mostly with the application of expandable balloon stents (Ref 1). However, the application of Nitinol stents in the femoral arteries has recently been considered by a few researchers (Ref 1, 2). Nitinol stents are exploited in the femoral arteries because of their self-expandable form, favorable radial force and ability to recover after crushing (Ref 1, 2).

The benefits of the application of Nitinol stent can be summarized as follows:

- effective contour-ability to obtain satisfactory fixation to the artery's wall;
- acceptable resistance against elastic recoil;
- fatigue resistance owing to pulsatile flow on body's kinematics;
- size minimization capability of the device for facilitating the percutaneous procedure; and
- low thrombogenicity and high biocompatibility with human natural system (Ref 2-4).

Austenite to martensite phase transformation of Nitinol is categorized as a first-order conversion (Ref 3, 4). This change is diffusionless and reversible (Ref 3, 4). The superelasticity is caused by the stress-induced martensite (SIM) transformation from austenite to martensite at temperatures generally above A_f (Ref 4). Above the temperature range A_f to M_d, where M_d is defined as the upper limit for the existence of SIM, the material is anticipated to relieve strain-energy by a phase transformation under a critical load. As the temperature increases over A_f, it becomes rather more difficult to induce martensite by stress while the temperature approaches M_d. The plateau stresses and residual strain increase with increasing temperature accordingly (Ref 4). At high enough temperatures (i.e., $T > M_d$), the loading plateau associated with the SIM transformation is not observed; instead, the material remains stable as the austenite phase (Ref 4).

The performance of the well-known self-expanding Nitinol stent is based on its superelastic behavior (Ref 3, 4).Material properties like A_f temperature greatly affect clinical performance of the superelastic Nitinol stents (Ref 4-11). The amount of A_f depends on the required stiffness and the stenosis volume of the femoral artery (Ref 4, 6). Too low A_f temperature results in high stiffness and increases the radial resistive force (RRF) of the stent which, in turn, injures the wall of the artery (Ref 3, 4, 7). Low A_f temperature results in a short fatigue life (Ref 4, 7, 11).

Five stent geometries have been dealt with in different studies: woven, ring, helical spring and cells (both closed and open) (Ref 12, 13). Open-cell Z-shaped rings are divided into structural elements that contribute to the longitudinal flexibility of the stent. Periodically connected peak-to-peak designs are regularly used in self-expanding stents like the smart versions (Ref 12-14).

There are relatively few published studies on the analysis of Nitinol wire stents (Ref 15-21). The first report on the numerical study of the fatigue behavior of Nitinol stent has been presented by Whitcher (Ref 18). Petrini et al. (Ref 17) have observed good agreements between other researchers' experimental results with their numerical data calculated for crushing tests. Kleinstreuer et al. (Ref 5) offered a computational analysis of different Nitinol stent-graft material combinations for supporting abdominal aortic aneurysm (AAA).

F. Nematzadeh, Department of Materials Engineering, Faculty of Engineering, Arak University, 38156-88349 Arak, Iran; and Materials and Energy Research Center (MERC), 14155-4777 Tehran, Iran; and **S.K. Sadrnezhaad,** Department of Materials Science and Engineering, Sharif University of Technology, 11155-9466 Tehran, Iran. Contact e-mail: fardinnematzadeh@gmail.com.

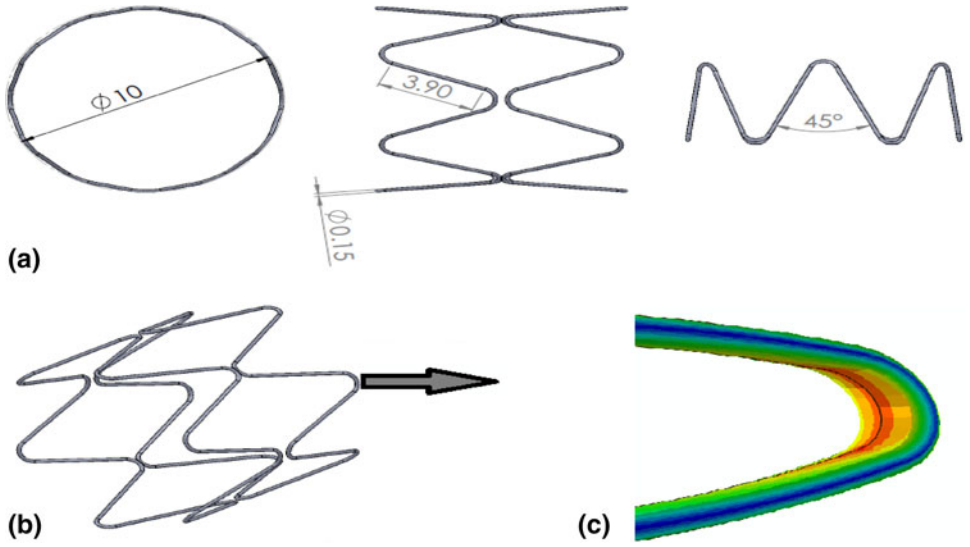

Fig. 1 Geometry of two-junction stent designed in this research. Different views are shown for better understanding of the shape: (a) geometric details, (b) full stent, and (c) exact position of the junction area of the stent where numerical calculations (the amount of maximum in curves of junction area) have been performed. Stent geometry at the junction as integrated is considered. Unit of length is mm

Table 1 Material properties used in simulation of femoral artery opening by Nitinol stent

Symbol	Description	Unit	Sample 1	Sample 2
E_A	Austenite elasticity	MPa	51,700	35,877
ν_A	Austenite Poisson's ratio		0.3	0.33
E_M	Martensite elasticity	MPa	47,800	24,462
ν_M	Martensite Poisson's ratio	…	0.3	0.33
ε^L	Transformation strain	…	0.063	0.055
$\left(\frac{\delta\sigma}{\delta T}\right)_L$	Stress/temperature ratio during loading	MPa/T	6.527	6.7
σ_L^S	Start of transformation loading	MPa	600	489
σ_L^E	End of transformation loading	MPa	670	572
T_0	Reference temperature	°C	37	22
$\left(\frac{\delta\sigma}{\delta T}\right)_U$	Stress/temperature ratio during unloading	MPa/T	6.527	6.7
σ_U^S	Start of transformation unloading	MPa	288	230
σ_U^E	End of transformation unloading	MPa	254	147
σ_{CL}^S	Start of transformation stress in compression	MPa	900	0.0
ε_V^L	Volumetric transformation strain	…	0.063	0.055
ε_{max}	Strain limit %	…	12	8
A_f	Austenite finish temperature	°C	20	32

The data are based on Auricchio model (5, 29)

Beule et al. (Ref 16) developed a strategy to investigate and optimize the mechanics of braided stents. Silber et al. (Ref 15) showed the effect of changing geometrical characteristic on the mechanical properties of the Nitinol wire stents. However, a numerical investigation of Z-shaped open-cell femoral artery self-expanding stents made of Nitinol wire is missing in the literature.

The present study provides a comprehensive evaluation of the effects of crimping and A_f temperature on mechanical performance of the Z-shaped open-cell self-expanding stent made of Nitinol wire when used in the femoral artery. The effects of the influential parameters are predicted via model calculations and are verified by empirical information available in the literature. The model was developed based on a nonlinear 3D finite element method (FEM). It is capable of determining the mechanical and clinical performance of the Z-shaped open-cell Nitinol self-expanding stent when implanted in the femoral artery.

The main purpose of the investigation was to employ the FEM for the evaluation of the impact of various crimping and A_f temperature values on the mechanical and clinical performance of the newly designed Nitinol stent for the femoral artery.

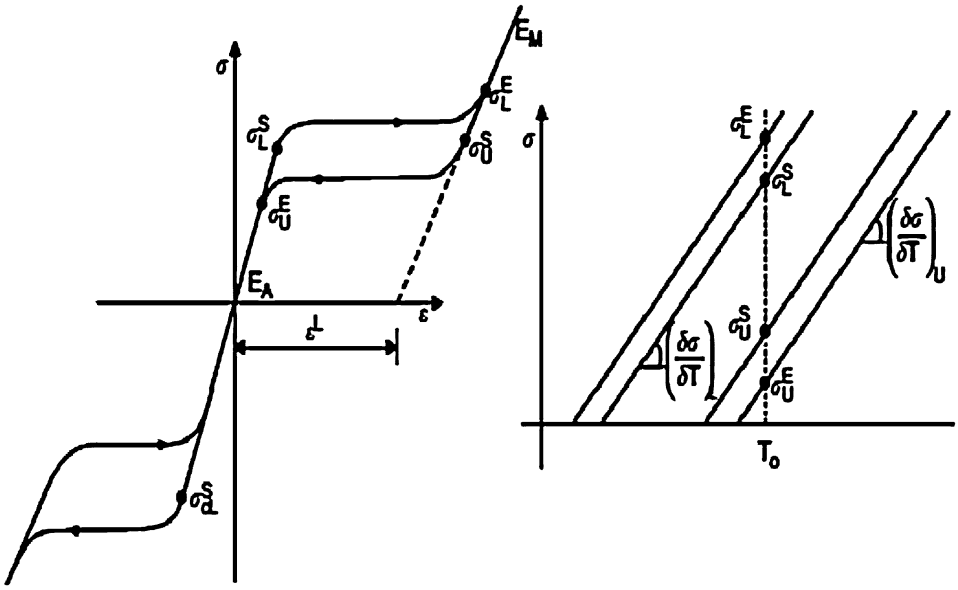

Fig. 2 Typical superelastic Nitinol behavior

Table 2 Mesh parameters of Nitinol stent for opening femoral artery during crimping

Material	Element type	Number of elements	Number of nodes
Stent	C3D8I	12,600	21,624
Crimper	SFM3D4	3,072	3,200

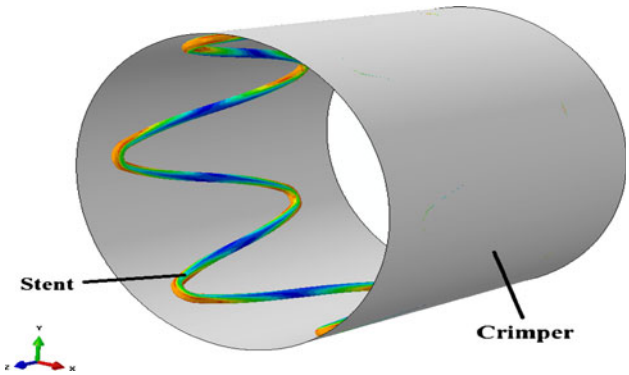

Fig. 3 Boundary conditions for the crimping of femoral artery stent

2. Material and Methods

2.1 Geometric Models

The geometries of the commercially made stents are based on restrictive patents. Little information has, therefore, been given by manufacturers about the effect of the geometry on the behavior of the stents. Therefore, Micro-CT should be used to obtain the optimum geometry. As an advantage of using this technique, it makes direct building of a 3D stent model possible. There are not enough information and clinical reports available in the literature describing NiTi femoral stent behavior. The present paper is to introduce a newly developed design of a SFA open-cell Z-shape wire stent usable for the treatment of the femoral occlusive disease.

Based on the information available in the literature (Ref 1, 2), a Nitinol stent with a new geometry, shown in Fig. 1, is designed for the femoral artery using the computer-aided three-dimensional interactive application (Catia v. 5, Dassault Systèmes, USA).

2.2 Material Properties

This study is focused on a comparison of material properties of Nitinol superelastic stents designed for the femoral artery. The model has originally been developed by Auricchio, Taylor, and Lubliner (Ref 22-24). The model modified by Rebelo is used for the simulation of Nitinol superelastic behavior (Ref 25, 26).

The model is based on the generalization of the theory of plasticity and thermodynamics of Helmholtz free energy, according to which strain is decomposed into two components:

$$\Delta\varepsilon = \Delta\varepsilon^{el} + \Delta\varepsilon^{tr} \quad \text{(Eq 1)}$$

where $\Delta\varepsilon^{el}$ is the linear elastic strain and $\Delta\varepsilon^{tr}$ is a transformation strain. Transformation of austenite to twinned martensite is driven by the motion of shear forces and takes place in the stress threshold range of the superelastic material according to the following equation:

$$F^S \leq F \leq F^F \quad \text{(Eq 2)}$$

In Eq 2, F is the transformation potential and S and F denote martensite transformation start and finish, respectively. A similar approach is applied to describe the reverse transformation which takes into account different stress thresholds.

$$\Delta\varepsilon^{tr} = a\Delta\zeta\frac{\partial F}{\partial\sigma} \quad \text{(Eq 3)}$$

$$\Delta\zeta = f(\sigma,\zeta)\Delta F \quad \text{(Eq 4)}$$

$$F = \bar{\sigma} - p\tan\beta + CT \quad \text{(Eq 5)}$$

where a is coefficient of strain, ζ is martensite fraction, σ is the Von Mises stress, $\bar{\sigma}$ is the Von Mises equivalent stress, p is pressure, β and C are material constants, and T is temperature.

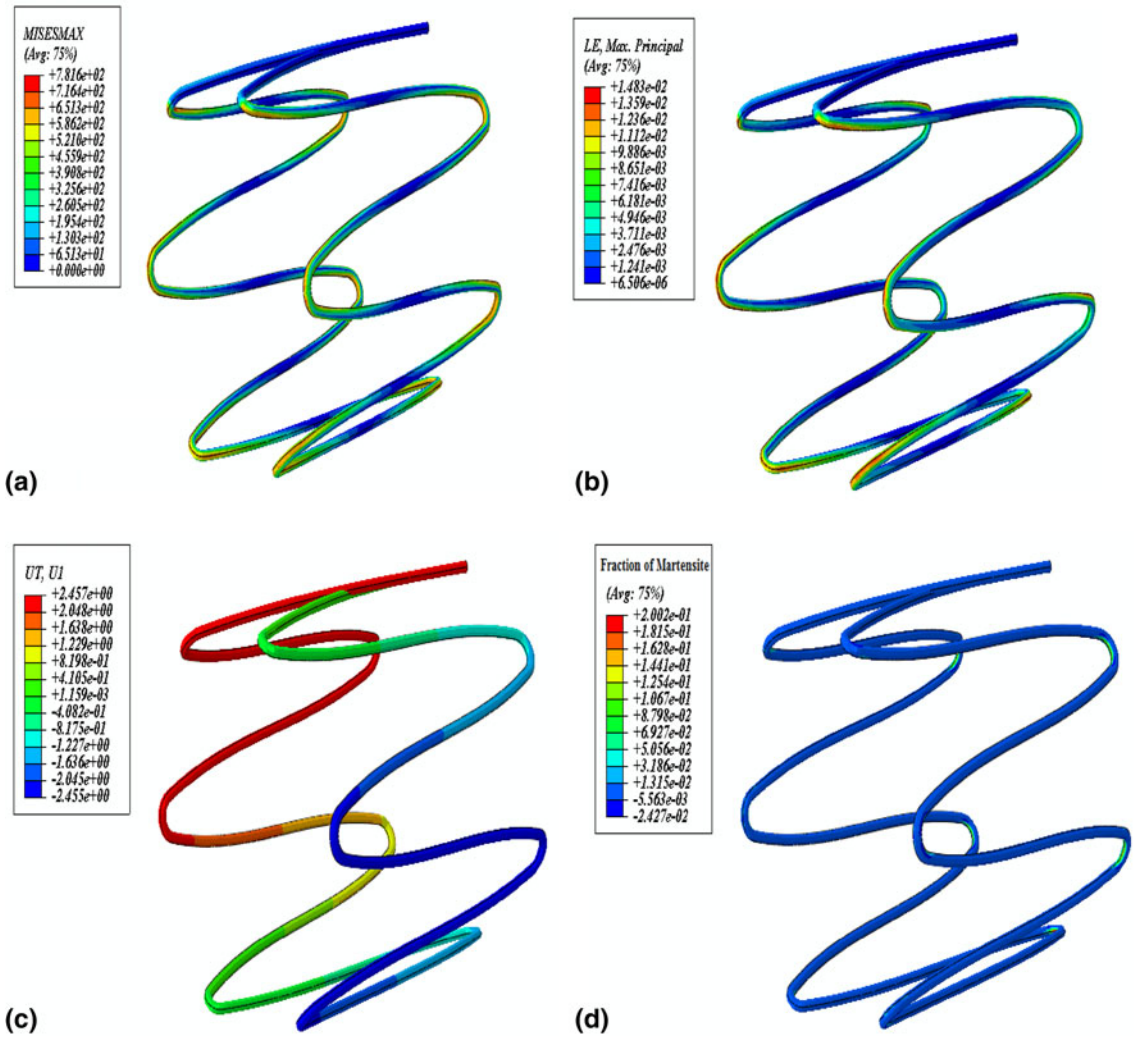

Fig. 4 Result of 50% crimping of Nitinol stents shown in Fig. 1 with material properties of Sample 1 of Table 1. (a) MISESMAX, (b) LEMAX, (c) U1, (d) Fraction of martensite

The intensity of the transformation follows a stress potential law according to Eq 3 and 4 (Ref 22-24).

Any changes in stress direction result in a martensite reorientation with negligible additional effort (Ref 22-25). Additionally, the model includes linear shifting of stress thresholds with temperature. Given the fact that there is a volume increase related to the transformation, less stress is required to produce transformation in tension, and more in compression. This effect is modeled by the linear Drucker-Prager approach for the transformation potential shown in Eq 5 (Ref 27, 28). Material properties defined in a subroutine are based on the Auricchio model (Ref 21-25). These are summarized in Table 1 (Ref 5, 29). Typical superelastic Nitinol behaviors are demonstrated in Fig. 2.

2.3 Meshing and Boundary Conditions

Owing to the complex geometry and small size of the wire section of the NiTi stent, Hypermesh software (Altair® Hypermesh® v. 6.0) is used for meshing of the samples. Mesh parameters of femoral Nitinol stent undergoing crimping test are listed in Table 2. In order to decrease the time of calculation and use the benefits of axis symmetry, only 1/4 size of geometrical models are analyzed. The temperature is set at 37 °C (body temperature).

The Finite element model should include the real boundary conditions applied on the stent (such as stent placement on surgical needle and its implant). Because of superelastic behavior of the Nitinol stent, the applied displacement process is suitable. With the above-mentioned conditions, the stent performance can be tested with the crimping experiment. Employing the ABAQUS /Standard v. 6.10 (Dassault Systèmes, Providence, RI, USA), only the contact between the outer stent surface and the inner cylindrical surface is activated. To perform the crimping test between the stent and the cylindrical surface (crimper) in both contraction and expansion steps, the surface-to-surface contact is assessed. Obviously, a cylindrical coordinate is better under these conditions with appropriate boundary conditions. Firstly, the contacts between the outer surface of the stent and the inner crimper surface are activated. In this contact algorithm, the master surface for the crimper and the slave surface for the stent is concurrently applied. Penalty is a general method for the evaluation of the contact with friction coefficients different in ABAQUS analysis. Such a contact is used to enforce impermeable boundaries. The surface contact between

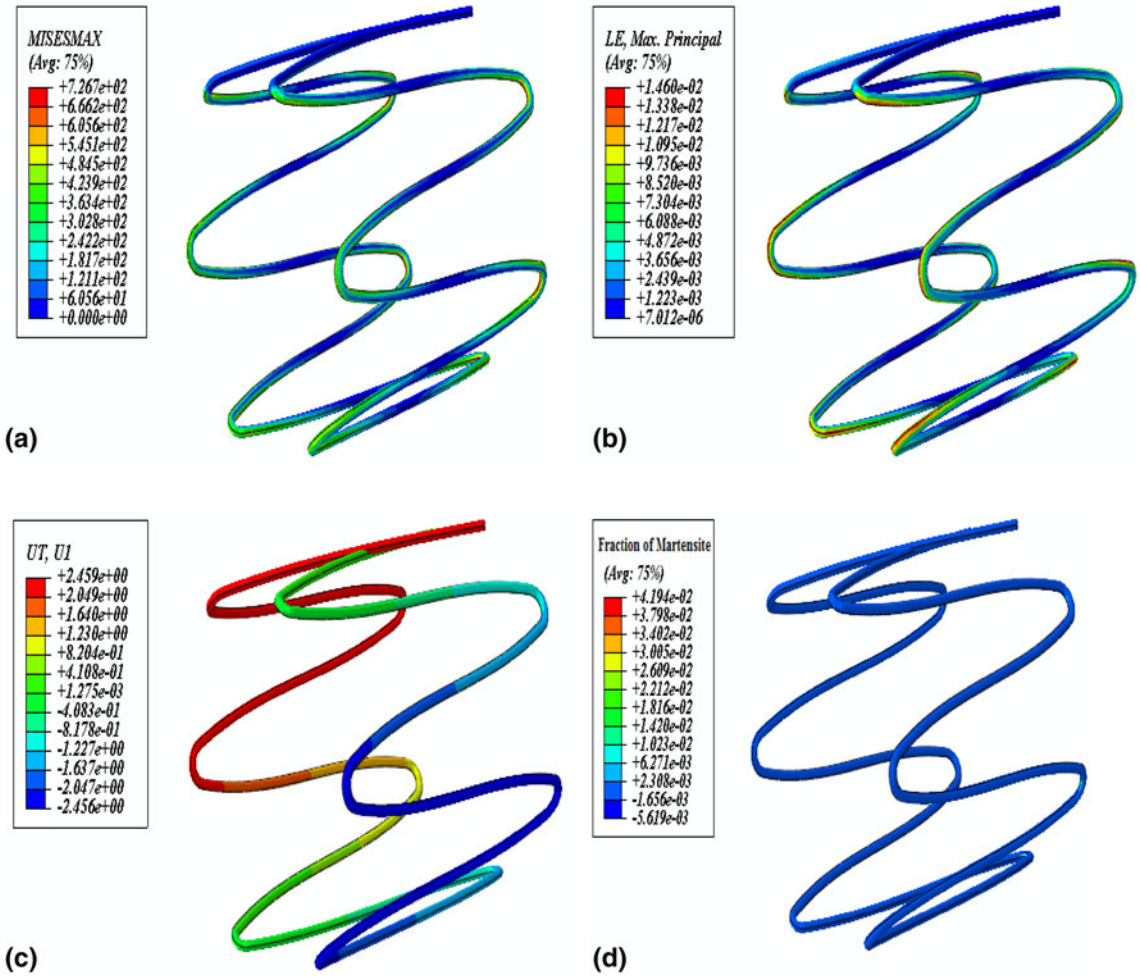

Fig. 5 Result of 50% crimping of Nitinol stents shown in Fig. 1 with material properties of Sample 2 of Table 1. (a) MISESMAX, (b) LEMAX, (c) U1, (d) Fraction of martensite

the crimper surface and flexible stent is considered to be frictionless. The boundary conditions are chosen so as to avoid the sliding of the stent in the crimper as well as to allow the stent deformation during crimping. Thus, the rotation of all components is inhibited and the stent is fixed in the axial direction at its end nodes. In the radial direction, the stent is permitted to deform without limitation under the crimping conditions. A radial displacement is enforced to the crimper and then, the stent shows its original shape after unloading. Fifty and sixty percent diameter reductions are applied by the crimper on the stent. The boundary conditions for the crimping of femoral artery stent are shown in Fig. 3.

3. Results

The Nitinol stents designed for the femoral artery is illustrated in Fig. 1. This paper first discusses the results of 50% and then, 60% crimping. Maximum Von Mises equivalent stress (MISESMAX), maximum logarithmic principal strain (LEMAX), spatial radial displacement (U1), and martensite fractional conversion caused by crimping of the Nitinol stent with material properties of samples 1 and 2 of Table 1 are shown in Fig. 4, 5, and 6. Comparison of Fig. 4, 5 and Table 3 indicates that the decrease in MISESMAX from 781.6 to 726.7 MPa results in a decrease in LEMAX from 0.0148 to 0.0146. The fraction of martensite reduces from 0.2 to 0.04 under the same conditions. The reduction ratio is approximately 1 and 79%, respectively. With the increase in the crimping level (U1) from 50 to 60%, as a comparison of Fig. 5, 6 and Tables 3, 4 shows, a decrease in MISESMAX from 726.7 to 716.8 MPa results in an increase in LEMAX from 0.0146 to 0.0174. The fraction of martensite increases from 0.04 to 0.17 under the same conditions. The increasing ratio is approximately 18 and 300%, respectively. Comparison of Fig. 4, 6 and Tables 3, 4 indicates that the decrease in MISESMAX from 781.6 to 716.8 MPa results in an increase in LEMAX from 0.0148 to 0.0174. The fraction of martensite reduces from 0.2 to 0.17 under the same conditions. The reduction ratio is approximately 15 %. Results of numerical calculations performed for the curved junction areas of Fig. 1c which are crimped under high pressure are shown in Fig. 7. According to Fig. 7, the increase in A_f temperature from 20 to 32 °C results in the reduction of the upper plateau stresses from 620 to 600 MPa. The reduction ratio is approximately 3%. Moreover, lower plateau stresses increase from 280 to 300 MPa under the same conditions. This increasing ratio is approximately 6%. Results of reference temperature

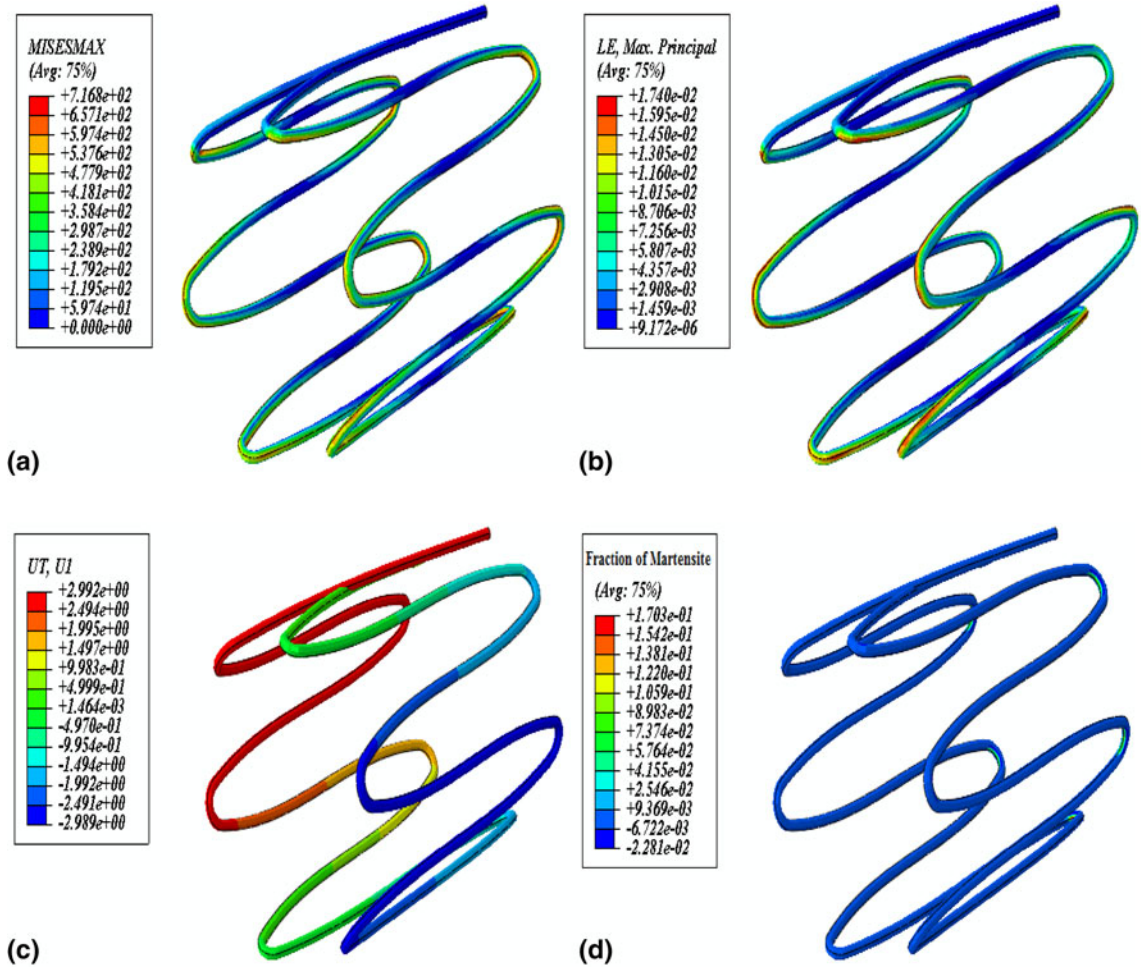

Fig. 6 Result of 60% crimping of Nitinol stents shown in Fig. 1 with material properties of Sample 2 of Table 1. (a) MISESMAX, (b) LEMAX, (c) U1, (d) Fraction of martensite

Table 3 Result of stress, strain, and fraction of Martensite of the femoral artery stent under 50% crimping

Stent models	MISESMAX, MPa	LEMAX	Fraction of Martensite
Sample 1 of Table 1	781.6	0.0148	0.2
Sample 2 of Table 1	726.7	0.0146	0.04

Table 4 Result of stress, strain, and fraction of Martensite of the femoral artery stent under 60% crimping

Stent models	MISESMAX, MPa	LEMAX	Fraction of Martensite
Sample 2 of Table 1	716.8	0.0174	0.17

mechanical testing are presented in Table 5. According to Table 5, comparison of sample No. 1 of Table 1 and sample No. 2 of Table 1 indicates that the decrease in the average of upper plateau strength from 635 to 530 MPa results in a significant reduction in the lower plateau strength from 271 to 188 MPa. This reduction ratio is approximately 30%.

4. Discussion

To evaluate Nitinol stents for the femoral artery, various parameters should be controlled such as mechanical hysteresis, chronic outward force (COF), RRF, the quality of plateau stress, stress distribution, strain distribution and the percentage of martensite (Ref 3-6). Nitinol stents for the femoral artery with the complete superelastic hysteresis loop, the lowest COF, the highest RRF, long plateau stress, lower stress and higher strain on critical points of the stent, and maximum fraction formation of martensite in the structure of the stent have shown the most favorable clinical performance (Ref 3-6, 30-32). COF and RRF are related to the superelastic behavior of the Nitinol stent. A classic superelastic stress-strain curve for the self-expanding stent is shown in Fig. 8. The stent is crimped by the cylindrical surface (path *a*-*b*), then later deployed, reaching a stress equilibrium with the artery at point *c*. The force against the artery is controlled by the COF and the force resisting deformation is controlled by the RRF. Usually, stent designers aim for as high RRF as possible with as low COF as possible (Ref 4, 12). Furthermore, two particular points should be considered (Ref 33-35): (1) the stents should observe SIM region of the stress-strain curve to show appropriate superelastic behavior; and (2) the stents should be in a failure-safe domain based on mechanical strength and strain. Based on the

studies in this field (Ref 5-11, 36-38), A_f temperature greatly affects the performance of Superelastic Nitinol stents.

The maintenance of optimal self-expanding Nitinol stent mechanical characteristics and full in vivo functionality, superelastic behavior between room temperature and body temperature is required (Ref 3, 4, 8). If the A_f temperature is higher, in some cases the SIM might not be complete and the stent no longer expands completely in the artery. At a lower A_f temperature, the plateau stresses are higher, which is especially unfavorable for the lower plateau (Ref 3, 4, 6-8).

Every Nitinol stent with high A_f temperature (close to body temperature) shows better fatigue life owing to low COF. A Nitinol stent is not required to high RRF for low stenosis of the femoral artery. The A_f temperature of the Nitinol stent for supplying high RRF should be much lower than the body temperature. The present study reveals that the A_f temperature is the dominant parameter and decreasing A_f temperature generally improves mechanical performance of the Nitinol stent for the femoral artery.

4.1 Evaluating the Effects of 50% Crimping on the Mechanical Performance of the Femoral Artery Stent

The MISESMAX on the internal curvature of the stent depicted in Fig. 4(a) is larger than that in Fig. 5(a); the latter is preferred to the former when considering the mechanical and clinical property aspects of designing these stents for use in the femoral artery. Furthermore, the LEMAX in the internal curvature of the stent illustrated in Fig. 5(b) is lower than that in Fig. 4(b), the latter possessing better dynamic motion and is in greater harmony with the femoral artery conditions. In addition, U1 (spatial radial displacement) of samples 1 and 2 indicated no noticeable difference because of equal crimping of the stents illustrated in Fig. 4(c) and 5(c). Moreover, the fractional conversion of austenite to martensite phase under stress in the internal curvature of the stent of Fig. 4(d) is higher than that in Fig. 5(d). Consequently, the Nitinol stent designed in Fig. 1 with material properties of sample 1 of Table 1 (with application of 50% crimping on the stent) is shown to have the best mechanical performance for the femoral artery stent, owing to the higher transformation strain related to the higher fraction of martensite formation, low stress and high strain in the internal curvature of the stent and more suitable superelastic behavior.

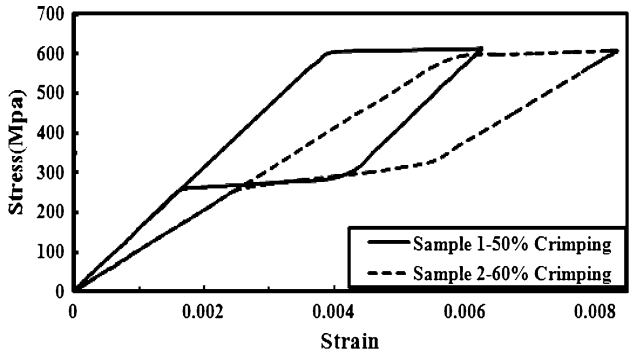

Fig. 7 Comparison between superelasticity behaviors resulted from 50 and 60% crimping of Nitinol stent shown in Fig. 1 with material properties of Samples 1 and 2 of Table 1

As mentioned previously, the stents should show the SIM region of the stress-strain curve in order to demonstrate suitable superelastic behavior (Ref 34, 35). A femoral Nitinol stent with material properties of sample 2 of Table 1 crimped with 50% deformation did not display the SIM transformation and was not suitable for the intended application.

4.2 Assessing the Effects of 60% Crimping on the Mechanical Performance of the Femoral Artery Stent

The MISESMAX on internal curvature of the stent depicted in Fig. 5(a) is larger than that of Fig. 6(a); the latter is preferred to the former when considering the mechanical and clinical property aspects of designing these stents for the application in the femoral artery. Additionally, the LEMAX in the internal curvature of the stent illustrated in Fig. 5(b) is lower than that of Fig. 6(b), the latter possessing better dynamic motion and is in greater harmony with the femoral artery conditions. Furthermore, U1 of sample 2 indicates a noticeable difference owing to 10% increase in crimping of the stents illustrated in Fig. 6(c). Moreover, fractional conversion of austenite to martensite phase under stress in the internal curvature of the stent of Fig. 6(d) is higher than that in Fig. 5(d).

As a result, the Nitinol stent designed in Fig. 1 with material properties of sample 2 of Table 1 (with application of 60% crimping on the stent) is shown to have the best mechanical

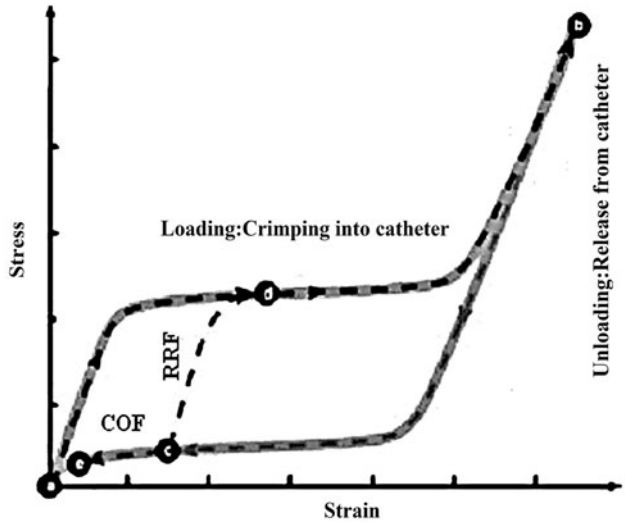

Fig. 8 Schematics of RRF and COF for a superelastic Nitinol stent

Table 5 Mean mechanical properties at reference temperature

Samples	A_f, °C	Average of Upper Plateau strength, MPa	Average of Lower Plateau strength, MPa	Transformation strain, %	Strain limit, %
Sample 1 of Table 1	20	635	271	6.3	12
Sample 2 of Table 1	32	530	188	5.5	8

performance for femoral artery stent owing to higher transformation strain related to higher fraction of martensite formation, less stress, more strain in the internal curvature of the stent and more suitable superelastic behavior.

The MISESMAX on internal curvature of the stent depicted in Fig. 4(a) is larger than that of Fig. 6(a); the latter is preferred to the former when considering the mechanical and clinical property aspects of designing these stents for the application in the femoral artery. In addition, the LEMAX in the internal curvature of the stent illustrated in Fig. 4(b) is lower than that of Fig. 6(b), the latter possessing better dynamic motion and is in greater harmony with the femoral artery conditions. Additionally, U1 of sample 2 indicates noticeable difference due to 10% increase in crimping of the stents illustrated in Fig. 6(c). Moreover, fractional conversion of austenite to martensite phase under stress in the internal curvature of the stent of Fig. 4(d) is higher than that in Fig. 6(d).

In conclusion, the Nitinol stent designed in Fig. 1 with material properties of sample 1 of Table 1 (bearing 50% crimping), according to Fig. 7, shows better mechanical and clinical performance due to higher fraction of martensite formation.

4.3 Assessing the Effects of A_f Temperatures on the Mechanical Performance of the Femoral Artery Stent

The changes in mechanical properties of Nitinol are closely linked to the changes in thermal properties by the Clausius-Clapeyron relationship (Ref 37-39):

$$\frac{d\sigma}{dT} = -\rho\frac{\Delta S f_m}{\varepsilon_t} = -\rho\frac{\Delta H f_m}{T_o\varepsilon_t} \quad \text{(Eq 6)}$$

where σ is the plateau stress, ε_t is the transformational strain, ΔH represents the enthalpy of the transformation per unit volume, ρ is the density of the transforming body, ΔS is the entropy change of the transformation, which is determined by the chemistry and crystallography of the transformation, T_o is the equilibrium temperature of the transformation, which is determined by the enthalpy and entropy changes of the transformation and f_m is the volume fraction of the transformation. The plateau strain associated with stress-induced martensitic transformation was found to increase with testing temperature, and hence with the increase in the critical stress. This is consistent with previous studies. It is also found that the increase in plateau strain does not affect the linearity of stress-temperature dependence, implying that the increase in ε_t was in proportion with an increase in f_m.

To ensure that the Nitinol self-expanding stents can recover to the designed shape when they are released from the delivery system, the A_f temperature of the Nitinol self-expanding stents should be lower than the body temperature (Ref 3-8). The A_f temperature of both samples introduced in Table 1 is below body temperature (37 °C). Two ΔT values were evaluated in this work. The ΔT was calculated as shown in the following equation:

$$\Delta T = (|T_{reference} - A_f|)$$

The temperature differences ranged from 17.0 to −10 °C.

The following graph in Fig. 7 plots the data from Table 5 to better represent the effect of test temperature on plateau stresses. There is an approximately 6% decrease in average plateau stresses in increasing the A_f temperature from 20 to 32 °C. Moreover, the material which exhibited better superelastic behavior was the one with smaller A_f temperature ($\Delta T = |17\ °C|$). The difference between the upper and lower plateau stresses is related to the A_f temperature. Also, the A_f temperature depends on the phase transformation temperature and the critical stress for the SIM transformation (Ref 8). A lower A_f temperature of Nitinol alloys and the extensive loading and unloading stress levels are related to the superelastic behavior of the used alloys. For an A_f temperature difference of 7 °C, there is approximately 50% increase in the stress level (Ref 3, 4). Moreover, reducing the A_f temperature increases the upper plateau stress (Ref 37). For an A_f temperature difference of 12 °C, the stress increase is approximately 4MPa in loading and unloading, and for each A_f temperature degree lower than the human body temperature, a 100% increase of stress is anticipated which is confirmed by experimental and numerical results (Ref 36-38).

According to Table 5, the transformation strain for sample No. 1 of Table 1 is 6.3%, which is much lower than the critical threshold value of 12% (strain limit), while sample No. 2 of Table 1 has a transformation strain of 5.55%, which is lower than its critical threshold value of 8% (strain limit). Thus, in terms of mechanical performance, sample No. 1 of Table 1 is preferable to sample No. 2 of Table 1.

According to Fig. 7, the stent with sample No. 2 of Table 1 shows poor performance in terms of the mechanical and clinical application owing to very high A_f temperature, small martensite fraction, and narrow hysteresis loop related to weak superelastic behavior. Consequently, based on desired clinical and mechanical standards of the stents and according to Fig. 7, the Nitinol stent designed in Fig. 1 with material properties of sample 1 of Table 1, with lower COF, higher RRF, higher transformation strain related to higher fraction of martensite formation, and a mechanical hysteresis loop indicating superelastic behavior shows the best performance from both mechanical and clinical viewpoints.

4.4 Limitations

Crimping simulations are too complicated due to contact points, nonlinear geometry, large deformation, sample buckling, stent bending, and stress-strain nonlinearity. On the contrary, the self-contact phenomenon is assumed only during contact between the edges of the stent in the crimping test (Ref 33). Owing to the superelastic behavior of the Nitinol stent, these contacts do not cause additional stress on the edges of the Nitinol stent. Crimping tests have only been performed in radial orientations (Ref 5, 15, 28, 31). It is obvious that more experiments and simulation results related to blood pressure, friction, type and gender of plaque, stenosis degree of artery and residual stresses are required to draw a comprehensive conclusion.

5. Conclusion

In this research, the effects of crimping and A_f temperature on mechanical and clinical performance of an open-cell Z-shaped femoral artery Nitinol stent is studied by crimping tests. Results show that A_f temperature is the dominant parameter. Decreasing A_f generally improves the mechanical performance of the stent. Calculations also show that increasing

A_f results in the increase in the COF and the decrease in the RRF, both of which affect forces of the stent. In particular, the Nitinol stent with A_f temperature of 20 °C and 50% crimping and having low COF, high RRF, elevated transformation strain related to large martensite fraction and mechanical hysteresis loop related to superelastic behavior shows the most desirable performance from both mechanical and clinical viewpoints.

Acknowledgments

The authors would like to thank Professor Amir R. Khoei, Ph.D., Civil Engineering Department, Sharif University of Technology and Mr. J. Arghavani, Ph.D., at Golpayegan College of Engineering, Iran for assisting the implementation of simulation program to modeled samples. We would also like to thank Mrs. A. Aghajani Koopaie, Ph.D. candidate at Mechanical Engineering Department of Iran University of Science and Technology for here invaluable advices about the numerical analysis of the stents.

References

1. J.M. Gibbs, C.S. Peña, and J.F. Benenati, Treating the Diseased Superficial Femoral Artery, *Tech. Vasc. Interv. Radiol.*, 2010, **13**, p 37–42
2. C.P. Cheng, G. Choi, R.J. Herfkens, and C.A. Taylor, The Effect of Aging on Deformations of the Superficial Femoral Artery Resulting from Hip and Knee Flexion: Potential Clinical Implications, *J. Vasc. Interv. Radiol.*, 2010, **21**, p 195–202
3. D. Stoeckel, A.R. Pelton, and T. Duerig, Self-expanding Nitinol Stents: Material and Design Considerations, *Eur. Radiol.*, 2004, **14**, p 296–301
4. T.W. Duerig, D.E. Tolomeo, and M. Wholey, An Overview of Superelastic Stent Design, *Minim. Invasive Ther. Allied Technol.*, 2000, **9**, p 235–246
5. C. Kleinstreuer, Z. Li, C.A. Basciano, S. Seeleckeand, and M.A. Farber, Computational Mechanics of Nitinol Stent Grafts, *J. Biomech.*, 2008, **41**, p 2370–2378
6. K. Koop, D. Lootz, C. Kranz, C. Momma, B. Becher, and M. Kieckbusch, Stent Material Nitinol—Determination of Characteristics and Component Simulation Using the Finite Element Method, *Prog. Biomed. Res.*, 2001, **6**, p 237–245
7. A.R. Pelton, T. Duerig, and D. Stockel, A Guide to Shape Memory and Superelasticity in Nitinol Medical Devices, *Minim. Invasive Ther. Allied Technol.*, 2004, **13**, p 218–221
8. X. Liu, Y. Wang, D. Yang, and M. Qi, The Effect of Ageing Treatment on Shape-Setting and Superelasticity of a Nitinol Stent, *Mater. Charact.*, 2008, **59**, p 402–406
9. E. Henderson, D.H. Nash, and W.M. Dempster, On the Experimental Testing of Fine Nitinol Wires for Medical Devices, *J. Mech. Behav. Biomed. Mater.*, 2011, **1**, p 1–8
10. Y. Liu and P. Galvin, Criteria for Pseudoelasticity in Near-equiatomic NiTi Shape Memory Alloys, *Acta Mater.*, 1997, **45**, p 4431–4439
11. A.R. Pelton, J. DiCello, and S. Miyazaki, Optimization of Processing and Properties of Medical Grade Nitinol Wire, *Minim. Invasive Ther. Allied Technol.*, 2000, **9**, p 107–118
12. D. Stoeckell, C. Bonsignore, and S. Duda, A Survey of Stent Designs, *Minim. Invasive Ther. Allied Technol.*, 2002, **11**, p 137–147
13. J. Zahora, A. Bezrouk, and J. Hanus, Models of Stents—Comparison and Applications, *Phys. Res.*, 2007, **56**, p S115–S121
14. B. Patrick, B.S. Snowhill, L.N. John, L.S. Randall, and H.S. Frederick, Characterization of Radial Forces in Z Stents, *Invest. Radiol.*, 2001, **36**, p 521–530
15. G. Silber, M. Alizadeh, and A. Aghajani, Finite Element Analysis for the Design of Self-expandable Nitinol Stent in an Artery, *Int. J. Energy Technol.*, 2010, **2**, p 1–7
16. M. De Beule, S.V. Cauter, P. Mortier, D.V. Loo, R.V. Impec, P. Verdonck, and B. Verhegghe, Virtual Optimization of Self-expandable Braided Wire Stents, *Med. Eng. Phys.*, 2009, **31**, p 448–453
17. L. Petrini, F. Migliavacca, P. Massarotti, S. Schievano, G. Dubini, and F. Auricchio, Computational Studies of Shape Memory Alloy Behavior in Biomedical Applications, *J. Biomech. Eng.*, 2005, **127**, p 716–725
18. F.D. Whitcher, Simulation of In Vivo Loading Conditions of Nitinol Vascular Stent Structures, *Comput. Struct.*, 1997, **64**, p 1005–1011
19. F. Migliavacca, L. Petrini, P. Massarotti, S. Schievano, F. Auricchio, and G. Dubini, Stainless and Shape Memory Alloy Coronary Stents: A Computational Study on the Interaction with the Vascular Wall, *Biomech. Model. Mechanobiol.*, 2004, **2**, p 205–217
20. P. Terriault, V. Brailovski, and R. Gallo, Finite Element Modeling of a Progressively Expanding Shape Memory Stent, *J. Biomech.*, 2006, **39**, p 2837–2844
21. F. Auricchio, M. Conti, M. De Beule, G. De Santis, and B. Verhegghe, Carotid Artery Stenting Simulation: From Patient-Specific Images to Finite Element Analysis, *Med. Eng. Phys.*, 2011, **33**, p 281–289
22. J. Lubliner and F. Auricchio, Generalized Plasticity and Shape Memory Alloy, *Int. J. Solid. Struct.*, 1996, **33**, p 991–1003
23. F. Auricchio and R. Taylor, Shape-Memory Alloys: Macromodeling and Numerical Simulations of the Superelastic Behavior, *Comput. Methods Appl. Mech. Eng.*, 1997, **146**, p 281–312
24. F. Auricchio and R.L. Taylor, Shape-Memory Alloys: Modeling and Numerical Simulations of the Finite-Strain Superelastic Behavior, *Comput. Methods Appl. Mech. Eng.*, 1996, **143**, p 175–194
25. N. Rebelo, N. Walker, and H. Foadian, Simulation of Implantable Stents, *Abaqus User's Conference*, Vol 143, 2001, p 421–434
26. M. Conti, M.D. Beule, P. Mortier, D.V. Loo, P. Verdonck, F. Vermassen, P. Segers, F. Auricchio, and B. Verhegghe, Nitinol Embolic Protection Filters: Design Investigation by Finite Element Analysis, *J. Mater. Eng. Perform.*, 2009, **18**, p 787–792
27. F. Auricchio, A. Coda, A. Reali, and M. Urbano, SMA Numerical Modeling versus Experimental Results: Parameter Identification and Model Prediction Capabilities, *J. Mater. Eng. Perform.*, 2009, **18**, p 649–654
28. J. Arghavani, F. Auricchio, R. Naghdabadi, and S. Sohrabpour, A 3-D Phenomenological Constitutive Model for Shape Memory Alloys Under Multiracial Loadings, *Int. J. Plast.*, 2010, **26**, p 976–991
29. M. Santillo, Fracture and Crack Propagation Study of a Superficial Femoral Artery Nitinol Stent, MS Thesis, Pavia University, 2008
30. F. Auricchio, M. Conti, S. Morganti, and A. Reali, Shape Memory Alloy: From Constitutive Modeling to Finite Element Analysis of Stent Deployment, *CMES*, 2010, **57**, p 225–243
31. M. Salaheldin, S.P. Zilla, and T. Franz, A Computational Study of Structural Designs for a Small-Diameter Composite Vascular Graft Promoting Tissue Regeneration, *Cardiovasc. Eng. Technol.*, 2010, **1**, p 269–281
32. V. Gideon, P. Kumar, and L. Mathew, Finite Element Analysis of the Mechanical Performance of Aortic Valve Stent Designs, *Trends Biomater. Artif. Organs*, 2009, **23**, p 16–20
33. W. Wu, M. Qi, X. Liu, D. Yang, and W. Wang, Delivery and Release of Nitinol Stent in Carotid Artery and Their Interactions: A Finite Element Analysis, *J. Biomech.*, 2007, **40**, p 3034–3040
34. X. Gong, T. Duerig, A.R. Pelton, N. Rebelo, and K. Perry, Finite Element Analysis and Experimental Evaluation of Superelastic Nitinol Stents, *SMST Conference*, 2003, p 453–462
35. A.R. Pelton, V. Schroeder, M.R. Mitchell, X.Y. Gong, M. Barneya, and S.W. Robertson, Fatigue and Durability of Nitinol Stents, *J. Mech. Behav. Biomed. Mater.*, 2008, **1**, p 153–164
36. K.W.K. Yeung, K.M.C. Cheung, W.W. Lu, and C.Y. Chung, Optimization of Thermal Treatment Parameters to Alter Austenitic Phase Transition Temperature of NiTi Alloy for Medical Implant, *Mater. Sci. Eng. A*, 2004, **383**, p 213–218
37. M. Patel, D. Plumley, and R. Bouthot, The Effects of Varying Active A_f Temperatures on the Fatigue Properties of Nitinol Wire, *ASM Materials Proceeding Conference*, MPMD, Boston, MA November, 2005, p 1–8
38. K. Otsuka and T. Kakeshita, Science and Technology of Shape Memory Alloys: New Developments, *MRS Bull.*, 2002, **27**, p 91–98
39. Y. Liu and H. Yang, Strain Dependence of the Clausius-Clapeyron Relation for Thermoelastic Martensitic Transformations in NiTi, *Smart Mater. Struct.*, 2007, **16**, p S22–S27